RSC Advances

PAPER

View Article Online
View Journal | View Issue

Cite this: *RSC Adv.*, 2025, **15**, 34939

Comprehensive study of organic–inorganic hybrid $[N(C_2H_5)_4]_2CdBr_4$: crystal structure, phase transitions, and structural geometry

Sun Ha Kim,[a] Daiha Shin,[a] Yoon-Joo Ko[b] and Ae Ran Lim *[cd]

The compound $[N(C_2H_5)_4]_2CdBr_4$, an organic–inorganic hybrid compound, has garnered attention for its potential applications across various fields. In this study, single crystals of $[N(C_2H_5)_4]_2CdBr_4$ were grown, and two distinct phase transition temperatures were identified: approximately 232 K (T_{C1}) and 476 K (T_{C2}). Single-crystal X-ray diffraction analysis at 300 K revealed a tetragonal structure belonging to the space group $P\bar{4}2_1m$. The thermal properties of the material were also briefly examined. Interestingly, while the ^{1}H NMR chemical shifts exhibited minimal variation around T_{C1}, the ^{13}C NMR spectra showed a noticeable change in the number of peaks, suggesting a structural phase transition. These observations indicate that the crystal retains a tetragonal structure above T_{C1} but transitions to a phase with lower symmetry below this temperature. Furthermore, ^{113}Cd NMR chemical shifts showed a significantly more pronounced change near T_{C1} compared to the shifts observed for ^{1}H and ^{13}C. This behavior reflects alterations in the local electronic environment around the Cd^{2+} ions, implying reconfiguration of the surrounding atomic framework. Additionally, the spin–lattice relaxation times for ^{1}H and ^{13}C, which are related to molecular motion, were nearly identical for both CH_2 and CH_3 groups in $[N(C_2H_5)_4]$ cations. The phase transition observed at T_{C1} is thus attributed to substantial structural rearrangements, particularly involving changes in atomic coordinates and the rotation of the $CdBr_4^{2-}$ tetrahedra.

Received 9th August 2025
Accepted 10th September 2025

DOI: 10.1039/d5ra05828g

rsc.li/rsc-advances

1. Introduction

Hybrid organic–inorganic metal halides have been extensively studied due to their promising applications in photovoltaic and optoelectronic devices. The broad range of applications and the rapid development of these materials have attracted significant attention from researchers.[1–12] In these compounds, the optical properties and structural flexibility are primarily governed by the organic cations, whereas the inorganic anions mainly determine their thermal and mechanical behavior. Their unique ability to combine the advantages of both organic and inorganic components makes them highly versatile for designing advanced functional materials.[13] Among these, the three-dimensional (3D) perovskite $CH_3NH_3PbI_3$ has recently received considerable interest due to its exceptional photovoltaic performance. However, its practical application is limited by its sensitivity to humidity and the toxicity associated with lead.[14–18] As a result, significant efforts have been directed toward the development of zero-dimensional (0D) hybrid organic–inorganic metal halides as more stable and less toxic alternatives. 0D hybrid metal halides with the general formula A_2MeX_4 have emerged as excellent candidates for phase-transition materials. In particular, tetraethylammonium-based compounds, $[N(C_2H_5)_4]_2MeX_4$ (where Me = Mn, Co, Cu, Zn, Cd and X = Cl, Br), belong to a large family of A_2MeX_4 crystals known to exhibit complex phase transitions influenced by both the metal (Me) and halide (X) ions.[19–53] These transitions are highly sensitive to external conditions due to hydrogen bonding between the molecular cations and the metal halide anions. Each $[N(C_2H_5)_4]^+$ cation resides in a cavity formed by surrounding MeX_4 anions, and many of these crystals undergo phase transitions involving rearrangements of both the MeX_4 units and the organic groups. The tetraethylammonium group itself can adopt two distinct stable conformations, with its ethyl chains offering greater configurational freedom compared to methyl-substituted analogs. While the nitrogen and terminal carbon atoms of the $[N(C_2H_5)_4]^+$ ion occupy well-defined positions, the central carbon atom can adopt two orientations, suggesting a disordered ionic configuration. More recently, attention has also turned to compounds that incorporate either mixed inorganic or organic components, such as $[N(C_2H_5)_4]_2CoCl_2Br_2$,[54–60] which contains mixed halides, and $[N(CH_3)_4][N(C_2H_5)_4]MeX_4$,[61–64] which features different organic cations.

[a]*Metropolitan Seoul Center, Korea Basic Science Institute, Seoul 03759, South Korea*
[b]*Laboratory of Nuclear Magnetic Resonance, National Center for Inter-University Research Facilities, Seoul National University, Seoul 08826, South Korea*
[c]*Graduate School of Carbon Convergence Engineering, Jeonju University, Jeonju 55069, Korea*
[d]*Department of Science Education, Jeonju University, Jeonju 55069, Korea. E-mail: aeranlim@hanmail.net; arlim@jj.ac.kr*

These systems offer further opportunities to explore structure–property relationships and design novel hybrid materials.

The $[N(C_2H_5)_4]_2CdBr_4$ compounds, the case where Me = Cd and X = Br, *i.e.*, has been reported in the literature only with respect to a few aspects. The transition temperature at 230 K was first reported by Kahrizi *et al.*[23] through capacitance dilatometry measurements. Vlokh *et al.*[25] investigated the optical birefringence of this single crystal and revealed a second-order phase transition at 118 K. Additionally, Sveleba *et al.*[29] reported a second-order phase transition at 311 K based on birefringence and dielectric experiments. Furthermore, changes in lattice parameters observed *via* X-ray diffraction suggested first-order phase transitions at 174 and 226 K, while an anomalous change was detected at 293 K.[44] In addition, Dekola *et al.*[45] demonstrated, through temperature-dependent heat capacity measurements, the occurrence of a first-order phase transition at 226.5 K. However, as shown in Table 1, these results are inconsistent with one another, and few detailed studies have been published on this compound to date. Although $[N(C_2H_5)_4]_2CdBr_4$ crystals have been relatively understudied among A_2MeX_4-type compounds, they have recently attracted attention due to their promising potential for practical applications.

In the present work, single crystals of $[N(C_2H_5)_4]_2CdBr_4$ were grown, and their phase transition behavior was investigated using differential scanning calorimetry (DSC) and powder X-ray diffraction (PXRD). The thermodynamic properties of the compound were briefly examined using thermogravimetric analysis (TGA) and differential thermal analysis (DTA). In addition, the crystal structure and lattice parameters at 300 K were determined by single-crystal X-ray diffraction (SCXRD) experiments. To examine the roles of $[N(C_2H_5)_4]^+$ cations and $CdBr_4^{2-}$ anions near the phase transition temperature, temperature-dependent chemical shifts in the ^1H, ^{13}C, and ^{113}Cd magic-angle spinning (MAS) nuclear magnetic resonance (NMR) spectra were analyzed. Moreover, spin–lattice relaxation times ($T_{1\rho}$) obtained from the NMR measurements were used to investigate molecular motion rates.

2. Experimental

2.1. Crystal growth

High-quality single crystals of $[N(C_2H_5)_4]_2CdBr_4$ were successfully grown using a slow evaporation method from supersaturated aqueous solutions. The crystals were obtained by dissolving tetraethylammonium bromide ($N(C_2H_5)_4Br$, Sigma-Aldrich, 99%) and cadmium bromide ($CdBr_2$, Sigma-Aldrich, 97%) in distilled water at a molar ratio of 2 : 1. The solution was thoroughly stirred and gently heated to achieve saturation, followed by gradual evaporation over several weeks in a constant-temperature bath maintained at 300 K. Several colorless and transparent single crystals with dimensions of approximately 5 × 4 × 3 mm were obtained. The resulting single crystals were carefully stored in a desiccator to prevent degradation caused by moisture exposure.

2.2. Characterization

Fourier-transform infrared (FT-IR) spectra were recorded in the range of 4000–500 cm^{-1} using a PerkinElmer L1600300 spectrometer (Waltham, MA, USA), with samples prepared as compressed KBr pellets. Differential scanning calorimetry (DSC) analyses were performed using a TA Instruments DSC system (Model 25) over the temperature range of 200–550 K, employing a heating rate of 10 K min^{-1} under a dry nitrogen atmosphere. The morphology of the crystals and their thermal evolution were monitored using a Carl Zeiss optical polarizing microscope equipped with a Linkam THM-600 heating stage. Thermogravimetric analysis (TGA) was carried out from 300 to 873 K at a heating rate of 10 K min^{-1} under a continuous flow of nitrogen gas.

The crystal structure and lattice parameters at 300 K were determined by single-crystal X-ray diffraction (SCXRD) analysis, conducted at Sookmyung Women's University using the Sookmyung Research Facilities. SCXRD data were obtained using a Bruker SMART CCD diffractometer equipped with a graphite-monochromated Mo-Kα radiation source. Data acquisition and integration were carried out using the SMART APEX3 and SAINT software suites, and absorption corrections were applied *via* the multiscan method implemented in SADABS.[65] Additionally, powder X-ray diffraction (PXRD) analysis was conducted using an Expert Pro-MPD X-ray diffractometer (PANalytical) fitted with Cu-Kα radiation and operated at 40 kV and 40 mA at the Korea Basic Science Institute (KBSI), Metropolitan Seoul Center. This instrumentation enabled the examination of the crystalline structure and phase composition of the samples. Furthermore, high temperature XRD analysis was performed utilizing an Anton Paar HTK 1200N stage coupled with the aforementioned

Table 1 The phase transition temperatures for previously reported $[N(C_2H_5)_4]_2CdBr_4$ crystals according to the various experimental methods

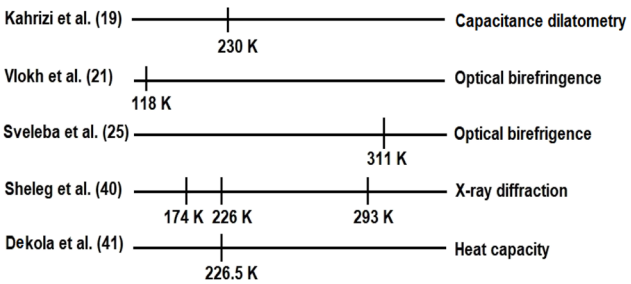

XRD system, allowing for the investigation of structural changes in the samples at elevated temperatures.

Solid-state ^{1}H and ^{13}C NMR spectra of $[N(C_2H_5)_4]_2CdBr_4$ were acquired using Bruker NMR spectrometers operating at 400 MHz and 500 MHz (Germany) at the Metropolitan Seoul Center of the KBSI and the NCIRF at Seoul National University, respectively. The ^{1}H magic angle spinning (MAS) NMR experiments were conducted at a Larmor frequency of 400.13 MHz, while the ^{13}C MAS spectra were recorded at 100.61 MHz and 125.77 MHz. Chemical shifts for both nuclei were referenced to tetramethylsilane (TMS). To minimize spinning sidebands, the MAS rate was set to 5 kHz. One-dimensional ^{1}H and ^{13}C spectra were collected with delay times of 5 s and 10 s, respectively. Spin–lattice relaxation times in the rotating frame ($T_{1\rho}$) were measured using a $\pi/2$ pulse followed by a spin-lock pulse of varying duration *t*. $T_{1\rho}$ values for ^{1}H and ^{13}C were determined with variable delay times ranging from 10 ms to 15 s. Additionally, ^{113}Cd MAS NMR chemical shifts were recorded at a Larmor frequency of 88.75 MHz, with $CdCl_2O_8\cdot 6H_2O$ serving as the reference compound. One-dimensional ^{113}Cd spectra were obtained using the one-pulse method with a delay time of 100 s. Temperature-dependent NMR measurements were carried out over the range of 180–430 K, with precise temperature control maintained by regulating the nitrogen gas flow and heating current.

3. Results and discussion

3.1. Fourier-transform infrared spectroscopy

The information related to FT-IR is presented in SI S1.

3.2. Phase transition temperature and thermodynamic properties

To determine the phase transition temperatures of $[N(C_2H_5)_4]_2CdBr_4$, single crystals were finely ground into powder using a mortar. Differential scanning calorimetry (DSC) measurements were conducted on approximately 8.5 mg of the sample at controlled heating and cooling rates of 10 K min^{-1}. As shown in Fig. 1, two endothermic peaks appeared during heating: a subtle peak near 232 K and a prominent peak around 476 K, corresponding to enthalpy changes of 246 J mol^{-1} and 15.15 kJ mol^{-1}, respectively. Upon cooling, a strong exothermic peak was observed at approximately 424 K, with an associated enthalpy change of 18.17 kJ mol^{-1}. These thermal transitions were found to be irreversible.

Complementary observations using optical polarizing microscopy revealed no significant morphological changes in the single crystals between 300 K and 513 K (see (a) and (b) within Fig. 1). At temperatures above this range, the initially colorless and transparent crystal became opaque (see (c) within Fig. 1), although no melting was observed up to approximately 600 K. This interpretation is further supported by subsequent powder X-ray diffraction (PXRD) analysis.

To investigate the thermal properties of $[N(C_2H_5)_4]_2CdBr_4$, thermogravimetric analysis (TGA) and differential thermal analysis (DTA) were carried out. As with the DSC measurements, the sample was finely ground into powder, and approximately 13.6 mg was used for analysis. The measurements were performed over the temperature range of 300–873 K at a heating rate of 10 K min^{-1}, consistent with the DSC conditions. As illustrated in Fig. 2, the TGA results indicated that the crystal remained thermally stable up to approximately 560 K, showing only a slight weight loss of about 2%. Partial thermal decomposition began at this point. Above the decomposition temperature (T_d) of 560 K, a significant weight loss was observed. The DTA curve exhibited two endothermic peaks, one near 476 K and another around 581 K. The peak at 476 K aligns well with that observed in the DSC results. In contrast, the peak at 581 K does not correspond to melting, as confirmed by polarizing microscopy, but rather indicates the onset of substantial sample decomposition. An inflection point observed at 662 K is attributed to the release of 2 equivalents of $[N(C_2H_5)_4]Br$, accounting for approximately 60% of the initial molecular weight, suggesting major thermal degradation. At temperatures exceeding 854 K, the sample showed nearly

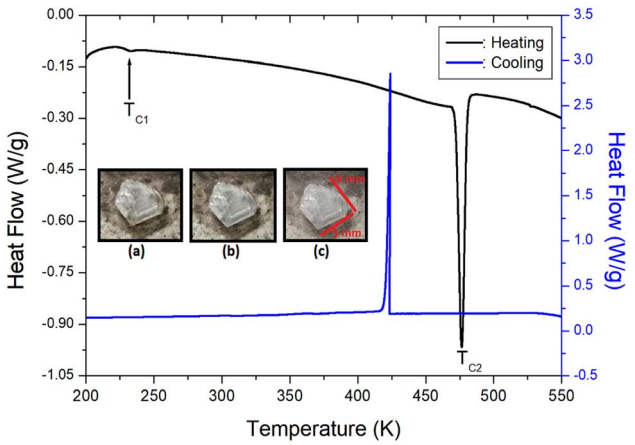

Fig. 1 Differential scanning calorimetry curves of $[N(C_2H_5)_4]_2CdBr_4$ measured at a heating and cooling rate of 10 K min^{-1} (inset: single crystal images at (a) 300 K, (b) 513 K, and (c) 583 K).

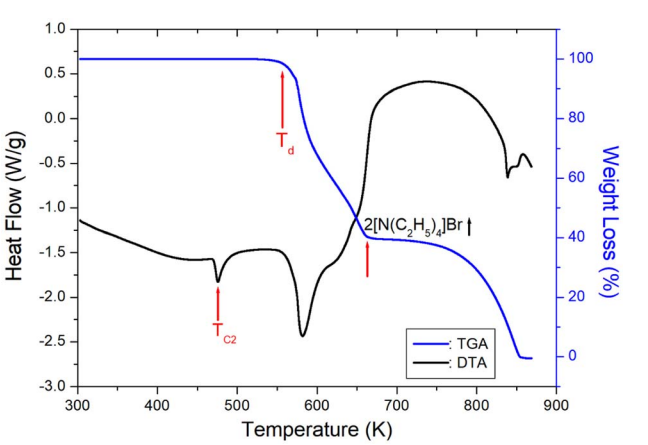

Fig. 2 Thermogravimetry and differential thermal analysis curves of $[N(C_2H_5)_4]_2CdBr_4$ measured at a heating rate 10 K min^{-1}. T_d is the decomposition temperature.

complete decomposition, with a total weight loss approaching 100%. These thermal analyses offer valuable insights into the compound's thermal stability, phase transition behavior, and decomposition profile.

3.3. X-ray diffraction experiment on single-crystal

Single-crystal X-ray diffraction (SCXRD) analysis was carried out on $[N(C_2H_5)_4]_2CdBr_4$ at 300 K. The compound crystallizes in the tetragonal system with space group $P\bar{4}2_1m$, and the lattice parameters were determined to be $a = b = 13.4605(3)$ Å, $c = 14.4058(4)$ Å, with $\alpha = \beta = \gamma = 90°$. The number of formula units per unit cell (Z) is 4, as summarized in SI S2. Fig. 3(a) and (b) depict the tetragonal crystal structure and thermal ellipsoids of each atom in $[N(C_2H_5)_4]_2CdBr_4$ at 300 K. Within the unit cell, two crystallographically distinct tetraethylammonium cations, denoted as $[N(1)(C_2H_5)_4]$ and $[N(2)(C_2H_5)_4]$, are present. The organic–inorganic framework consists of these cations and $CdBr_4^{2-}$ anions. A summary of selected bond-lengths and angles is provided in SI S3. The Cd–Br bond-lengths range from 2.582 Å to 2.587 Å, and the Br–Cd–Br bond angles vary between 107.69° and 112.58°, indicating a distorted tetrahedral coordination geometry around the Cd^{2+} ion. As also shown in SI S3, the distances from N(1) to its four surrounding carbon atoms range from 1.46 Å to 1.49 Å, while all four N(2)–C distances are uniformly 1.50 Å. This suggests that the local symmetry around N(2) is higher than that around N(1). The crystallographic information file (CIF) corresponding to the SCXRD data collected at 300 K is available in SI S4. Additionally, the complete crystallographic dataset has been deposited with the Cambridge Crystallographic Data Centre (CCDC 2477720). And, the morphology of the colorless and transparent single crystal grown in this study is shown in Fig. 3.

A simulated powder X-ray diffraction (PXRD) pattern generated from the CIF file closely agrees with the experimental PXRD pattern obtained from powdered $[N(C_2H_5)_4]_2CdBr_4$ samples, as shown in Fig. 4. Notably, two prominent diffraction peaks were observed at 11.09° and 13.15°, corresponding to the (111) and (200) plane, respectively. Peak indexing was carried out using the Mercury software. Powder X-ray diffraction (PXRD)

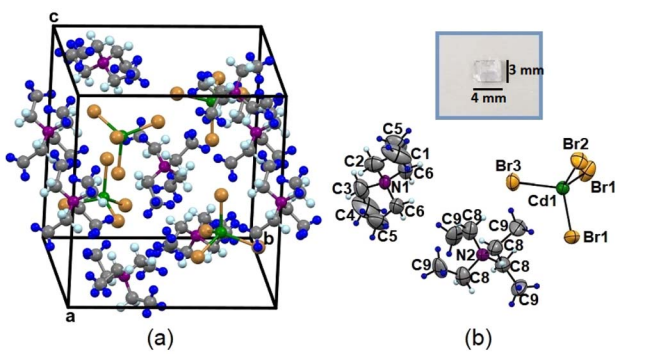

Fig. 3 (a) Tetragonal structure and (b) thermal ellipsoids for two type of $[N(C_2H_5)_4]$ cations and $CdBr_4$ anion of $[N(C_2H_5)_4]_2CdBr_4$ crystal at 300 K (inset: morphology of a colorless and transparent single crystal at 300 K) (CCDC no. 2477720).

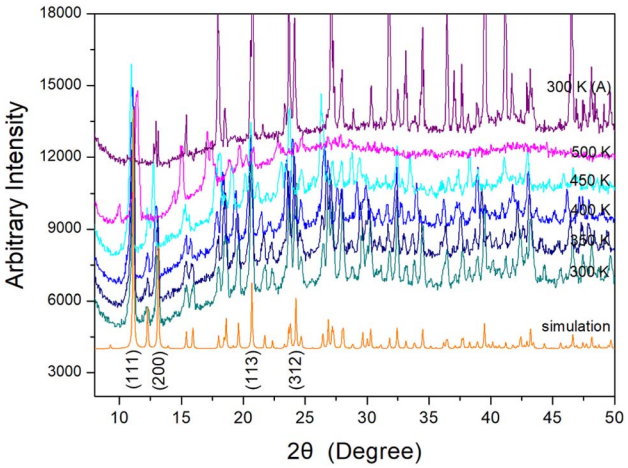

Fig. 4 Powder X-ray diffraction (PXRD) patterns with temperature variation and the simulated XRD pattern of $[N(C_2H_5)_4]_2CdBr_4$. The 300 K (A) pattern represents the PXRD pattern measured after cooling the single crystal from 500 K to 300 K.

measurements were conducted on crushed single crystals of $[N(C_2H_5)_4]_2CdBr_4$ over a 2θ range of 8–50° at temperatures above 300 K, and the results are presented in Fig. 5. The diffraction patterns recorded below 450 K remained nearly identical, indicating that the crystal structure is stable within this temperature range. In contrast, a clear change in the PXRD pattern was observed at 500 K, which corresponds well with the endothermic peak near 476 K identified in the DSC analysis. Furthermore, the presence of well-defined diffraction peaks at 500 K suggests the formation of a new crystalline phase rather than melting. The PXRD pattern obtained at 300 K after cooling the sample from 500 K (denoted as 300 K (A)) showed a significant difference compared to the original 300 K pattern. This indicates that the structural change is irreversible, in agreement

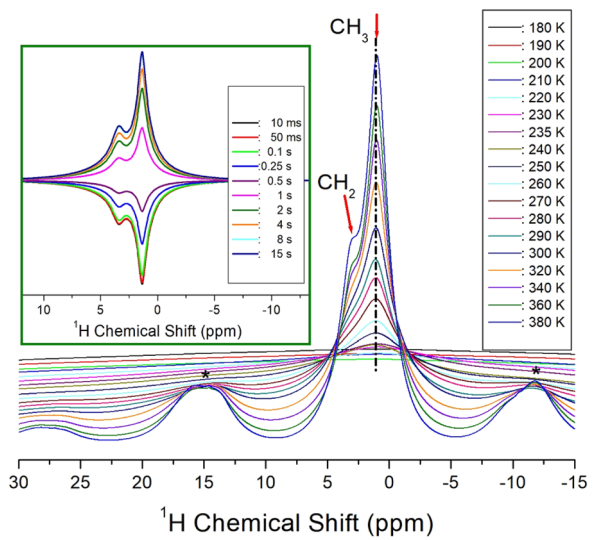

Fig. 5 ^1H NMR spectra for CH_2 and CH_3 in $[N(C_2H_5)_4]_2CdBr_4$ with increasing temperature (inset: recovery traces measured with the delay time of 10 ms–15 s).

with the DSC results. Based on the combined evidence from DSC and PXRD analyses, the phase transition temperatures of $[N(C_2H_5)_4]_2CdBr_4$ are estimated to be approximately 232 K (T_{C1}) and 476 K (T_{C2}).

3.4. ^{1}H MAS NMR chemical shifts and spin–lattice relaxation times

The ^{1}H MAS NMR spectra of $[N(C_2H_5)_4]_2CdBr_4$ single crystals were recorded at a Larmor frequency of 400.13 MHz under a 9.4 T magnetic field to investigate structural changes near T_{C1}. Tetramethylsilane (TMS) was used as an external reference for accurate calibration of chemical shifts. The spectra, acquired at a spinning rate of 5 kHz, are presented in Fig. 5. Peaks marked with asterisks (*) correspond to spinning sidebands, located approximately ±12.5 ppm from the central peak, consistent with the 5 kHz MAS rate. Below T_{C1}, the spectrum exhibits a single resonance, whereas above T_{C1}, two partially overlapping signals become apparent. At 300 K, signals at 1.04 ppm and 2.91 ppm are assigned to the protons of the CH_3 and CH_2 groups, respectively. The signal at 1.04 ppm shows significantly higher intensity than the one at 2.91 ppm, consistent with the relative number of hydrogen atoms in the CH_3 and CH_2 groups. Overall, the ^{1}H chemical shifts exhibit minimal variation with temperature, indicating weak temperature dependence.

At 300 K, the spin–lattice relaxation time $T_{1\rho}$ value for ^{1}H in $[N(C_2H_5)_4]_2CdBr_4$ was determined, and the recovery trace of nuclear magnetization can be well described by a single exponential function, as expressed by the following equation:[66,67]

$$P(t) = P(0)\exp(-t/T_{1\rho}) \quad (1)$$

In this context, $P(t)$ denotes the magnetization measured after a spin-lock period of duration t, whereas $P(0)$ represents the initial magnetization prior to spin-locking. The ^{1}H MAS NMR spectra were acquired at 300 K by varying the spin-lock delay time. The resulting signals, obtained over a delay range of 10 ms to 15 s, are shown in the inset of Fig. 5, and the decay of magnetization follows the exponential behavior described by eqn (1). From the slope of the magnetization decay curves, the spin–lattice relaxation time in the rotating frame ($T_{1\rho}$) was determined. The $T_{1\rho}$ values for the CH_3 and CH_2 groups were found to be identical, each measuring 2.68 s.

3.5. ^{13}C MAS NMR chemical shifts and spin–lattice relaxation times

The ^{13}C MAS NMR spectra of $[N(C_2H_5)_4]_2CdBr_4$ were recorded at resonance frequencies of 100.61 MHz and 125.77 MHz under magnetic fields of 9.4 T and 11.7 T, respectively. Tetramethylsilane (TMS) was used as the external reference to ensure accurate chemical shift calibration. At 300 K and a spinning speed of 10 kHz, two distinct signals were observed at 54.24 ppm and 10.30 ppm, corresponding to the CH_2 and CH_3 carbon environments, respectively. The temperature dependence of the ^{13}C chemical shifts was examined at a reduced spinning rate of 5 kHz for both Larmor frequencies, as presented in Fig. 6. The square and triangle symbols in the plot

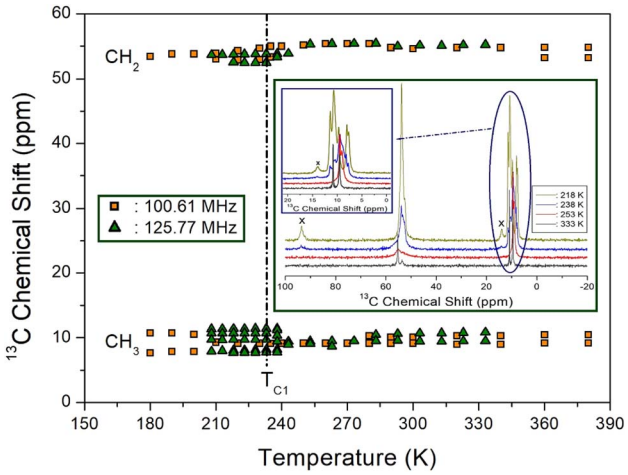

Fig. 6 ^{13}C NMR chemical shifts for CH_2 and CH_3 in $[N(C_2H_5)_4]_2CdBr_4$ measured at Larmor frequency of 100.61 and 125.77 MHz with increasing temperature (inset: ^{13}C NMR spectra at 218, 238, 253, and 333 K).

represent data obtained at 100.61 MHz and 125.77 MHz, respectively, and show good agreement. Due to instrumental limitations, low- and high-temperature spectra were not acquired at 10 kHz, as such conditions could impose excessive mechanical stress on the MAS NMR probe. Overall, the ^{13}C chemical shifts exhibited minimal variation with increasing temperature. However, below the T_{C1} transition temperature, the spectra for both CH_3 and CH_2 groups displayed splitting into multiple peaks. As the temperature increased and approached T_{C1} (*e.g.*, at 238 K), the split signals began to merge; above T_{C1}, only one or two signals were observed, as illustrated in the inset of Fig. 6. The peak labeled "x" near 54 ppm is a spinning sideband associated with the CH_2 group. At 218 K, well below T_{C1}, the CH_3 signal is split into several distinct peaks, indicating reduced symmetry. This spectral behavior suggests that the local structural environment around the ^{13}C nuclei is less symmetric at lower temperatures and becomes more symmetric above T_{C1}.

The spin–lattice relaxation time in the rotating frame ($T_{1\rho}$) for ^{13}C nuclei in $[N(C_2H_5)_4]_2CdBr_4$ at 300 K was determined using eqn (1), following a method analogous to that used for the ^{1}H $T_{1\rho}$ measurements. The ^{13}C MAS NMR spectra were analyzed by tracking changes in signal intensity as a function of delay time. Spectral data collected over a delay range of 10 ms to 15 s are shown in Fig. 7. The $T_{1\rho}$ values were extracted from the slopes of the magnetization recovery curves. As a result, the $T_{1\rho}$ values for the CH_2 and CH_3 carbon atoms were found to be very similar, measured at 2.13 s and 2.14 s, respectively.

3.6. ^{113}Cd MAS NMR chemical shifts

The ^{113}Cd MAS NMR experiments were performed across a temperature range encompassing the phase transition temperature T_{C1}, in order to gain insight into the coordination environment of the Cd^{2+} ion within the $CdBr_4^{2-}$ anion. The temperature-dependent ^{113}Cd chemical shifts, measured at

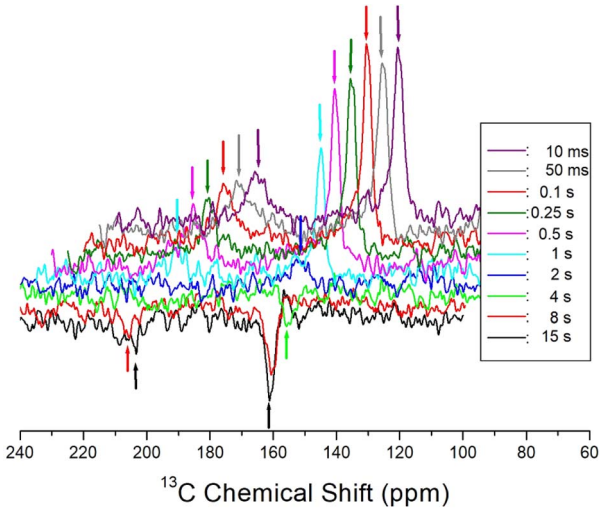

Fig. 7 ^{13}C NMR recovery traces in $[N(C_2H_5)_4]_2CdBr_4$ measured with the delay time of 10 ms–15 s at 300 K.

a Larmor frequency of 88.75 MHz, are presented in Fig. 8. The chemical shift and line width in the ^{113}Cd NMR spectrum as a function of temperature are shown in detail in Fig. 9. The ^{113}Cd resonance shifts toward lower (more negative) values with increasing temperature, exhibiting an abrupt discontinuity near T_{C1}. Specifically, the chemical shift changes from approximately 392 ppm at 180 K below T_{C1} to around 362 ppm at 380 K above this transition, suggesting a structural modification in the local environment surrounding the Cd^{2+} ion. Similarly, the line width follows a temperature-dependent trend analogous to that of the chemical shift. Notably, a pronounced narrowing of the line width occurs near T_{C1}, decreasing sharply from roughly 15 ppm below T_{C1} to approximately 1.3 ppm at 380 K. The narrowing of the ^{113}Cd line widths with increasing temperature suggests an enhanced mobility of the ^{113}Cd nuclei. This significant reduction implies enhanced dynamic behavior of the Cd^{2+} ion, which

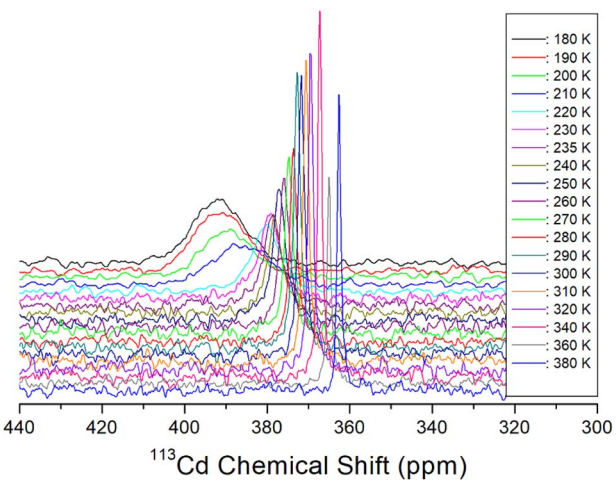

Fig. 8 ^{113}Cd NMR spectra in $[N(C_2H_5)_4]_2CdBr_4$ with increasing temperature.

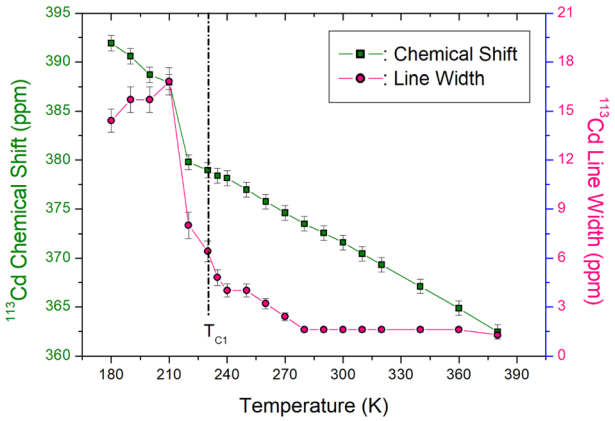

Fig. 9 ^{113}Cd NMR chemical shifts and line widths in $[N(C_2H_5)_4]_2CdBr_4$ near the phase transition temperature T_{C1}.

is tetrahedrally coordinated by four Br^- ions, at elevated temperatures.

4. Conclusions

Colorless and transparent single crystals of $[N(C_2H_5)_4]_2CdBr_4$ were grown *via* an aqueous solution method. Differential scanning calorimetry and related analyses revealed two phase transition temperatures at approximately 232 K (T_{C1}) and 476 K (T_{C2}). The compound crystallizes in a tetragonal system with space group $P\bar{4}2_1m$, and demonstrates thermal stability up to approximately 560 K. On the other hand, although the ^{1}H MAS NMR chemical shifts showed minimal variation near T_{C1}, the ^{13}C MAS NMR spectra exhibited notable changes in peak multiplicity across this temperature, indicating a lowering of symmetry below T_{C1}. This suggests that while the crystal maintains tetragonal symmetry above T_{C1}, it transitions to a lower-symmetry phase at lower temperatures. Furthermore, ^{113}Cd MAS NMR spectra revealed more pronounced changes near T_{C1} compared to those of ^{1}H and ^{13}C. The change in chemical shifts with temperature indicates a change in local electronic configuration at the ^{113}Cd sites, which in turn means that the neighboring atoms change their configurations. The line width behavior is consistent with increased rotational freedom of the $CdBr_4^{2-}$ tetrahedra upon phase transition; the changing line widths are attributed to various internal molecular motions. Additionally, spin–lattice relaxation times in the rotating frame ($T_{1\rho}$) for both CH_3 and CH_2 groups were found to be nearly identical: 2.68 s for ^{1}H and 2.14 s for ^{13}C. This similarity implies comparable molecular mobility for both functional groups across the transition. The phase transition in the $[N(C_2H_5)_4]_2CdBr_4$ crystal occurs at $T_{C1} = 232$ K and is accompanied by distinct structural changes, primarily due to variations in atomic coordinates and the rotation of the $CdBr_4^{2-}$ tetrahedra. A detailed investigation of the structural and physical properties of this organic–inorganic hybrid compound will demonstrate its potential for various technological applications in the future.

Author contributions

A. R. Lim performed crystal growth and wrote the manuscript. S. H. Kim and Y.-J. Ko measured NMR experiments, and D. Shin measured X-ray experiments.

Conflicts of interest

There are no conflicts to declare.

Data availability

CCDC 2477720 contains the supplementary crystallographic data for this paper.[68]

All relevant data are within the manuscript and the SI. See DOI: https://doi.org/10.1039/d5ra05828g.

Acknowledgements

This research was supported by the Regional Innovation System & Education (RISE) program through the Jeonbuk RISE Center, funded by the Ministry of Education (MOE) and the Jeonbuk State, Republic of Korea (2025-RISE-13-JJU).

References

1 Y.-F. Gao, T. Zhang, W.-Y. Zhang, Q. Ye and D.-W. Fu, Great advance in high T_c for hybrid photoelectric-switch bulk/film coupled with dielectric and blue-white light, *J. Mater. Chem. C*, 2019, **7**, 9840.

2 S. K. Abdel-Aal, A. S. Abdel-Rahman, W. M. Gamal, M. Abdel-Kader, H. S. Ayoub, A. F. El-Sherif, M. F. Kandeel, S. Bozhko, E. Yakimov and E. B. Yakimov, Crystal structure, vibrational spectroscopy and optical properties of a one-dimensional organic–inorganic hybrid perovskite of $[NH_3CH_2CH(NH_3)CH_2]BiCl_5$, *Acta Crystallogr., Sect. B*, 2019, **75**, 880.

3 N. Mahfoudh, K. Karoui, F. Jomni and A. B. Rhaiem, Structural phase transition, thermal analysis, and spectroscopic studies in an organic–inorganic hybrid crystal: $[(CH_3)_2NH_2]_2ZnBr_4$, *Appl. Organomet. Chem.*, 2020, **34**, e5656.

4 Y. Xie, Y. Ai, Y.-L. Zeng, W.-H. He, X.-Q. Huang, D.-W. Fu, J.-X. Gao, X.-G. Chen and Y.-Y. Tang, The Soft Molecular Polycrystalline Ferroelectric Realized by the Fluorination Effect, *J. Am. Chem. Soc.*, 2020, **142**, 12486.

5 D.-W. Fu, J.-X. Gao, W.-H. He, X.-Q. Huang, Y.-H. Liu and Y. Al, High-T_c Enantiomeric Ferroelectrics Based on Homochiral Dabco-derivatives (Dabco =1,4-Diazabicyclo [2.2.2]octane), *Angew. Chem., Int. Ed.*, 2020, **59**, 17477.

6 C. Su, M. Lun, Y. Chen, Y. Zhou, Z. Zhang, M. Chen, P. Huang, D. Fu and Y. Zhang, Hybrid Optical-Electrical Perovskite Can Be a Ferroelastic Semiconductor, *CCS Chem.*, 2021, **4**, 2009.

7 S. K. Abdel-Aal, M. F. Kandeel, A. F. El-Sherif and A. S. Abdel-Rahman, Synthesis, Characterization, and Optical Properties of New Organic–Inorganic Hybrid Perovskites $[(NH_3)_2(CH_2)_3]CuCl_4$ and $[(NH_3)_2(CH_2)_4]CuCl_2Br_2$, *Phys. Status Solidi A*, 2021, **218**, 2100036.

8 S. K. Abdel-Aal and A. Ouasri, Crystal structure, Hirshfeld surfaces and vibrational studies of tetrachlorocobaltate hybrid perovskite salts $NH_3(CH_2)_nNH_3CoCl_4$ (n = 4, 9), *J. Mol. Struct.*, 2022, **1251**, 131997.

9 Y.-L. Zeng, X.-Q. Huang, C.-R. Huang, H. Zhang, F. Wang and Z.-X. Wang, Unprecedented 2D homochiral hybrid lead-iodide perovskite thermochromic ferroelectrics with ferroelastic switching, *Angew. Chem., Int. Ed.*, 2021, **60**, 10730.

10 J.-Q. Gan, Z.-K. Xu, T. Gan, Y. Qin and Z.-X. Wang, Large phase-transition temperature enhancement achieved in a layered lead iodide hybrid crystal by H/F substitution, *Inorg. Chem.*, 2023, **62**, 14469.

11 L. long, Z. Huang, Z.-K. Xu, T. Gan, Y. Qin, Z. Chen and Z.-X. Wang, H/F substitution activating tunable dimensions and dielectric-optical properties in organic lead-bromide hybrids, *Inorg. Chem. Front.*, 2024, **11**, 845.

12 J.-Y. Yu, Z.-K. Xu, J.-Q. Gan, Y. Qin, H.-P. Lv and Z.-X. Wang, Beryllium-based ABX3-type organic-inorganic hybrid halide ferroelastic, *Inorg. Chem.*, 2025, **64**, 5284.

13 M. F. Mostafa and A. Hassen, Phase transition and electric properties of long chain Cd(II) layered perovskites, *Phase Transitions*, 2006, **79**, 305.

14 X. N. Hua, W. Q. Liao, Y. Y. Tang, P.-F. Li, P. P. Shi, D. Zhao and R. G. Xiong, A Room-Temperature Hybrid Lead Iodide Perovskite Ferroelectric, *J. Am. Chem. Soc.*, 2018, **140**, 12296.

15 A. Kojima, K. Teshima, Y. Shirai and T. Miyasaka, Organometal halide perovskites as visible-light sensitizers for photovoltaic cells, *JACS Commun.*, 2009, **131**, 6050.

16 T. M. Koh, *et al.*, Formamidinium-containing metal-halide: An alternative material for near-IR absorption perovskite solar cells, *J. Phys. Chem. C*, 2014, **118**, 16458.

17 Y. H. Khattak, E. Vega, F. Baig and B. M. Soucase, Performance investigation of experimentally fabricated lead iodide perovskite solar cell via numerical analysis, *Mater. Res. Bull.*, 2022, **151**, 111802.

18 A. Babayight, A. Ethirajan, M. Muller and B. Conings, Toxicity of organometal halide perovskite solar cells, *Nat. Mater.*, 2016, **15**, 247.

19 G. D. Stucky, J. B. Folkers and T. J. Kistenmacher, The crystal and molecular structure of tetraethylammonium tetrachloro-nickelate (II), *Acta Crystallogr.*, 1967, **23**, 1064.

20 T. P. Melia and R. Merrifield, Thermal properties of transition-metal compounds. part II. complexes of manganese, Iron, Cobalt, Nickel, Copper, and Zinc of the type $(Net_4)_2MCl_4$, *J. Chem. Soc. A*, 1970, 1166.

21 J. N. Mcelearney, G. E. Shankle, R. W. Schwartz and R. L. Carlin, Low-temperature magnetic characteristics of tetrahedral $CoCl_4^{2-}$. II. Nature of the phase transition in $[(C_2H_5)_4N]_2CoCl_4$, *J. Chem. Phys.*, 1972, **56**, 3755.

22 A. J. Wolthuis, W. J. Huiskamp, L. J. de Jongh and R. L. Carlin, Investigation of structural phase transitions in some $[(C_2H_5)_4N]_2MX_4$ compounds, with M = Co, Zn, Mn, and X = Cl, Br, *Physica B*, 1986, **142**, 301.

23 M. Kahrizi and M. O. Steinitz, Structural phase transitions in $((C_2H_5)_4N)_2CdX_4$ compounds with X = Cl, Br, *Solid State Commun.*, 1989, **70**, 599.
24 M. Kahrizi and M. O. Steinitz, Thermal expansion and phase transitions in some tetra-alkylammonium metal chlorides, *Solid State Commun.*, 1990, **74**, 333.
25 O. G. Vlokh, I. I. Polovinko, V. I. Mokryi and S. A. Sveleba, Optical birefringence of single crystals of $[N(C_2H_5)_4]_2ZnBr_4$ and $[N(C_2H_5)_4]_2CdBr_4$, *Sov. Phys. Crystallogr.*, 1991, **36**, 131.
26 M. Iwata and Y. Ishibashi, Dielectric dispersion in $[N(C_2H_5)_4]_2ZnCl_4$ single crystal, *J. Phys. Soc. Jpn.*, 1991, **60**, 3245.
27 Z. Czapla and S. Dacko, Structural phase transitions in $[(C_2H_5)_4N]_2MX_4$ crystals, *Ferroelectrics*, 1992, **125**, 17.
28 T. Kawata, T. Aoyama and S. Ohba, Tetraethylammonium tetrachlorocuprate (II), $[N(C_2H_5)_4]_2[CuCl_4]$, *Acta Crystallogr., Sect. C: Cryst. Struct. Commun.*, 1993, **49**, 137.
29 S. Sveleba, V. Morkyi, I. Polovinko, V. Kapustyanik and Z. Trybula, Birefringent and dielectric properties of $[N(C_2H_5)_4]_2ZnBr_4$ and $[N(C_2H_5)_4]_2CdBr_4$ crystals, *Acta Phys. Pol. A*, 1993, **83**, 777.
30 O. Caetano, M. Lopez, A. Mahoui, J. Lapasset, J. Moret, T. Assih and P. S. Gregoire, Structural instabilities in the $(TEA)_2$ m Cl_4 crystalline family: A DSC study, *Ferroelectr. Lett.*, 1995, **19**, 69.
31 A. Mahoui, J. Lapasset, J. Moret and P. S. Gregoire, Structure of $(TEA)_2CuCl_4$ and hydration, *Z. Kristallogr.*, 1995, **210**, 125.
32 A. Mahoui, J. Lapasset, J. Moret and P. S. Gregoire, Bis (tetraethylammonium) Tetrachlorometallates, $[(C_2H_5)_4N]_2[MCl_4]$, where M=Hg, Cd, Zn, *Acta Crystallogr., Sect. C: Cryst. Struct. Commun.*, 1996, **52**, 2671.
33 A. Mahoui, J. Lapasset, D. G. Sannikov, J. Moret and P. S. Gregoire, On the ordering in $[(C_2H_5)_4N]_2CuCl_4$ crystal: an X-ray study and theoretical considerations, *Z. Phys. B*, 1996, **99**, 543.
34 Z. Tylczynski and P. Biskupski, Low-temperature dielectric dispersion in $[N(C_2H_5)_4]_2CuCl_4$ crystal, *Solid State Commun.*, 1997, **102**, 385.
35 M. Machida, T. Ishino, Y. Shimoikeda, S. Gondo, N. Kotano and Y. Iwata, NMR and X-ray investigations of phase transition in $[N(C_2H_5)_4]_2ZnCl_4$, *Ferroelectrics*, 1998, **217**, 105.
36 Z. Tylczynski and P. Biskupski, Thermal properties of $[N(C_2H_5)_4]_2CuCl_4$, *J. Korean Phys. Soc.*, 1998, **32**, S235.
37 R. Poprawski, A. Liber and E. Malek, Dilatometric investigations of overcritical behavious in $[N(C_2H_5)_4]_2CuCl_4$ crystals, *Acta Phys. Pol. A*, 2000, **98**, 61.
38 Z. Tylczynski, P. Biskupski and M. Slaboszewska, Dielectric dispersion in $[N(C_2H_5)_4]_2MeCl_4$ crystals, *Ferroelectrics*, 2002, **272**, 315.
39 M. A. Kandhaswamy and V. Srinivasan, Synthesis and characterization of tetrarthylammonium tetrachlorocobaltate crystals, *Bull. Mater. Sci.*, 2002, **25**, 41.
40 K. Gesi, Effect of hydrostatic pressure on the phase transitions in $[N(C_2H_5)_4]_2CuCl_4$, *Ferroelectrics*, 2003, **285**, 139.
41 P. Biskupski, M. Slaboszewska and Z. Tylczynski, Changes in the optical properties at phase transitions in TEA_2MeCl_4 (Me = Zn, Mn, Hg, Cu) crystals, *Phys. B*, 2005, **370**, 6.
42 A. U. Sheleg, A. M. Natumovets, T. I. Dekola and N. P. Tekhanovich, Effect of γ irradiation on the structural and thermal properties of $[N(C_2H_5)_4]_2ZnBr_4$ in the vicinity of a first-order phase transition, *Phys. Solid State*, 2006, **48**, 354.
43 M. Maczka, A. Cizman, R. Poprawski and J. Hanuza, Temperature-dependent vibrational studies of $[N(C_2H_5)_4]_2MnCl_4$, *J. Raman Spectrosc.*, 2007, **38**, 1622.
44 A. U. Sheleg, E. M. Zub and A. Y. Yachkovskii, Crystallographic characteristics and phase transitions in the $[N(C_2H_5)_4]_2CdBr_4$ crystal in the low-temperature range, *Phys. Solid State*, 2007, **49**, 1973.
45 T. I. Dekola, A. U. Sheleg and N. P. Tekhanovich, Heat capacity of the $[N(C_2H_5)_4]_2CdBr_4$ crystal in the temperature range 80-300 K, *Phys. Solid State*, 2007, **49**, 1766.
46 A. R. Lim and K.-Y. Lim, Phase-transition mechanisms of $[N(C_2H_5)_4]_2BCl_4$ and $[N(CH_3)_4]_2BCl_4$ (B=^{63}Cu and ^{67}Zn) single crystals studied by proton NMR, *Solid State Commun.*, 2008, **147**, 11.
47 P. Biskupski and Z. Tylczynski, Structure of TEA_2ZnCl_4 crystal surfaces studied by AFM, *Phase Transitions*, 2008, **81**, 971.
48 A. Ostrowski and A. Cizman, EPR studies of linewidth anomalies at phase transitions in $[N(C_2H_5)_4]_2MnCl_4$, *Physica B*, 2008, **403**, 3110.
49 A. R. Lim, Study on ethyl groups with two different orientations in $[N(C_2H_5)_4]_2CuBr_4$, *J. Phys. Chem. Solid.*, 2016, **93**, 59.
50 A. R. Lim, Study of the ferroelastic phase transition in the tetraethylammonium compound $[N(C_2H_5)_4]_2ZnBr_4$ by magic-angle spinning and static NMR, *AIP Adv.*, 2016, **6**, 035307.
51 A. R. Lim, M. S. Kim and K.-Y. Lim, Nuclear magnetic resonance study of the ferroelastic phase transition of order-disorder type $[N(C_2H_5)_4]_2CdCl_4$, *Solid State Sci.*, 2016, **58**, 101.
52 A. R. Lim and K.-Y. Lim, Structural changes near phase transition temperatures for the $[N(C_2H_5)_4]$ groups in hydrated $[N(C_2H_5)_4]_2CuCl_4 \cdot xH_2O$, *J. Therm. Anal. Calorim.*, 2017, **130**, 879.
53 M. B. Bechir and A. B. Rhaiem, Synthesis, Thermal Analysis, Optical, Electric Properties and Conduction Mechanism of Hybrid Halogenometallates: $[N(C_2H_5)_4]_2CoCl_4$, *J. Phys. Soc. Jpn.*, 2021, **90**, 74709.
54 V. Kapustianik, I. Polovinko, Yu. Korchak, S. Sveleba, R. Tchukvinskyi and S. Kaluza, Phase transitions in $[N(C_2H_5)_4]_2MeCl_2Br_2$ (Me=Zn, Co, Cu) solid solutions, *Phys. Status Solidi A*, 1997, **161**, 515.
55 V. Kapustianyk, Y. Shchur, I. Kityk, V. Rudyk, G. Lach, L. Laskowski, S. Tkaczyk, J. Swiatek and V. Davydov, Resonance dielectric dispersion of TEA-$CoCl_2Br_2$ nanocrystals incorporated into the PMMA matrix, *J. Phys.: Condens. Matter*, 2008, **20**, 365215.

56 V. Kapustianyk, Ya. Shchur, I. Kityk, V. Rudyk, G. Lach, L. Laskowski, S. Tkaczyk, J. Swiatek and V. Davydov, Resonance dielectric dispersion of TEA-$CoCl_2Br_2$ nanocrystals incorporated into the PMMA matrix, *J. Phys.: Condens. Matter*, 2008, **20**, 365215.

57 V. Kapustianyk, V. Rudyk, P. Yonak and B. Kundys, Magnetic and dielectric properties of $[N(C_2H_5)_4]_2CoClBr_3$ solid solution: A new potential multiferroic, *Phys. Status Solidi B*, 2015, **252**, 1778.

58 V. Kapustianyk, B. Cristovao, D. Osypiuk, Yu. Eliyashevskyy, Yu. Chornii and B. Sadovyi, Magnetic and ferroelectric properties of new potential magnetic multiferroic $[N(C_2H_5)_4]_2CoCl_2Br_2$, *Acta Phys. Pol. A*, 2021, **140**, 450.

59 V. Kapustianyk, Yu. Eliyashevskyy, U. Mostovoi, S. Semak, R. Tarasenko, V. Tkac, A. Feher and E. Cizmar, The correlation between electric polarization and magnetic properties in $[N(C_2H_5)_4]_2CoCl_2Br_2$ crystal at low temperatures, *Physica B*, 2022, **646**, 414299.

60 Z. Wu, H. Tang, T. Dai, Y. Long, D. Luo, P. Jiang, X. Xiong, Y. Xu, X. Zhang and Q. Hu, Mixed-ligand Engineering to enhance luminescence of Mn^{2+}- based metal halides for wide color gamut display, *materials*, 2024, **17**, 4459.

61 N. Izumi, Dielectric properties of $N(CH_3)_4N(C_2H_5)_4CoBr_4$ crystal, *J. Phys. Soc. Jpn.*, 1996, **65**, 1189.

62 F. Hlel, A. Rheim, T. Guerfel and K. Guidara, Synthesis, calorimetric study, infrared spectroscopy and crystal structure investigation of β-[tetraethylammonium tetramethylammonium tetrachlorozincate (II)] [β]-$[(C_2H_5)_4N][(CH_3)_4N]ZnCl_4$, *Z. Naturforsch.*, 2006, **61b**, 1002.

63 E. Bozkurt, I. Ucar, I. Kartal, B. Karabulut and Y. Bekdemir, Structural, spectroscopic and EPR studies of tetraethlyammonium tetraethylammonium tetrabromocuprate (II) complex, *Z. Kristallogr.*, 2009, **224**, 163.

64 K. Karoui, A. B. Rhaiem, F. Hlel, M. Arous and K. Guidara, Dielectric and electric studies of the $[N(CH_3)_4][N(C_2H_5)_4]ZnCl_4$compound at low temperature, *Mater. Chem. Phys.*, 2012, **133**, 1.

65 *SMART and SAINT-Plus v6.22*, Bruker AXS Inc., Madison, Wisconsin, USA, 2000.

66 J. L. Koenig, *Spectroscopy of Polymers*, Elsevier, New York, 1999.

67 A. Abragam, *The Principles of Nuclear Magnetism*, Oxford University Press, 1961.

68 S. H. Kim, D. Shin, Y.-J. Ko and A. R. Lim, CCDC 2477720: Experimental Crystal Structure Determination, 2025, DOI: **10.5517/ccdc.csd.cc2p58gm**.